THE JOURNAL OF PHYSICAL CHEMISTRY C

pubs.acs.org/JPCC Article

Mineral Dissolution under Electric Stimulation

Yi-Hsuan Hsiao, Xin Chen, Erika Callagon La Plante, Aditya Kumar, Mathieu Bauchy, Dante Simonetti, David Jassby, Jacob Israelachvili, and Gaurav Sant*

Cite This: *J. Phys. Chem. C* 2020, 124, 16515−16523

Read Online

ACCESS | Metrics & More | Article Recommendations

ABSTRACT: Although mineral dissolution and precipitation have been extensively studied, the role of electric stimulation on these processes remains unclear. We reveal the effects of *subcritical electric potential* (i.e., lower than the breakdown potential of water) on the bulk dissolution rates of calcite (carbonate; $CaCO_3$) using a custom-built three-electrode cell. The effects of applied potential depend on the pH, ionic strength, and temperature. For calcite, the enhancement in dissolution rates—under isothermal conditions—is explained by enhanced ion transport. Thus, at acidic to near-neutral pH (pH 4−6) wherein calcite's dissolution is mass transfer or mixed mode controlled, dissolution rates increase with increasing potential. But, under alkaline conditions (pH 10), wherein surface reactions limit calcite's dissolution, its dissolution rate is unaffected by electric potential. This suggests that subcritical applied potentials do not appear to alter the distribution of charged surface sites within the inner Helmholtz plane (IHP) of the electric double layer (EDL) at the mineral−solution interface. Rather, applied potential acts to enhance transport-controlled dissolution by enhancing the ion flux in to and out of the diffusion boundary layer (DBL). This results in a reduction in the activation energy of mineral dissolution in proportion to the applied potential, indicating a Butler−Volmer mechanism of dissolution stimulation. This mechanism is confirmed by comparison to orthoclase ($KAlSi_3O_8$), which dissolves exclusively under surface control—whose dissolution is unaffected by applied potential. As a result, applied potentials are only effective when the mass transfer of ions is the rate-limiting step of mineral dissolution.

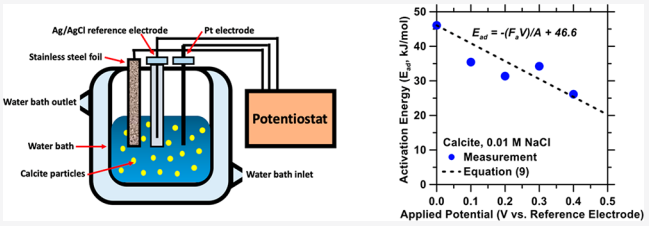

INTRODUCTION AND BACKGROUND

The dissolution of minerals is relevant to both natural and engineered environments. For instance, mineral dissolution rates have been measured to understand sedimentary rock evolution,[1] seawater pH,[2] neutralization of acidic lakes,[3] decadal natural weathering processes,[3] and synthetic approaches for ocean alkalinity enhancement.[4,5] Calcite's ($CaCO_3$) dissolution and precipitation have been the subject of many of these studies. In addition to its natural prevalence, calcite also has industrial applications including as an electrolyte in mineral-based fuel cells (i.e., solid oxide fuel cell (SOFCs)),[6−8] in electrokinetic remediation,[9] in the manufacture of phosphatic fertilizers,[10,11] and as a construction material.[12]

The rates and mechanisms of calcite's dissolution are strongly affected by the solvent's pH, solution saturation state, the abundance and type of co-ions present in solution, and its ionic strength and temperature.[13−17] While the vast majority of studies have examined passive approaches for affecting mineral dissolution rates, less is known, for example, of how active stimulation as induced by an electric field may affect dissolution behavior. Some studies have shown how electric potential-induced acidification of the solvent in the proximity of the anode can enhance calcite's (and other mineral's) dissolution rates.[18,19] Other than the pioneering studies of Kristiansen et al.[20] and Dobbs et al.,[21] comparatively less is known, however, of how potential-induced ion transport and changes in the structure of the electric double layer (EDL) that is present at the mineral−water interface may affect mineral dissolution, particularly at subcritical potentials (i.e., at ambient temperatures, water dissociates for $\Delta V \geq 1.23$ V), wherein water's acidification can be excluded.

Conceptual Basis. Mineral dissolution consists of two concurrent processes: (1) the dissolution reaction at the interface between the solid and the liquid (i.e., surface reaction) and (2) the diffusion of reactive species (i.e., dissolved ions, ions from electrolyte solutions) to and from this interface (i.e., mass transport/transfer), i.e., across a diffusion boundary layer (DBL).[22] The slower of these two processes establishes the rate-limiting step of dissolution. The dissolution of limestone (87 wt % calcite) for 2 < pH < 6 is controlled by proton diffusion to the solid surface ("mass transfer control").[23] On the other hand, at near-neutral to mildly

Received: May 28, 2020
Revised: July 2, 2020
Published: July 2, 2020

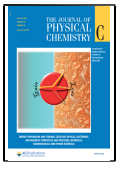

https://dx.doi.org/10.1021/acs.jpcc.0c04823
J. Phys. Chem. C 2020, 124, 16515−16523

alkaline pH, calcite's dissolution is controlled by a combination of surface reactions and mass transport, i.e., "mixed kinetic control", and under (hyper)alkaline conditions surface reactions control dissolution, i.e., dissolution is "surface reaction controlled".[13,24]

At the surface termination, in a vacuum, bare calcite (and the vast majority of condensed solids) is electrically neutral. However, in general, as a solute's surface contacts a solvent (or liquid water, broadly speaking), in circumstances wherein charged species may form/be present/exist, an EDL forms at the solute (mineral)−solvent (water) interface on account of the (i) specific adsorption of ions and (ii) Coulombic interaction forces, which attract/repel ions, in relation to the underlying native surface charge, such that in the limit the surface charge is *neutralized* with increasing distance from the surface, i.e., into the solution (see Figure 1).[25,26] In the case of calcite, when exposed to an aqueous solution, ion exchange at the calcite−water interface results in the formation of a net negatively charged compact layer of relatively immobile ions[27] that exist within the inner Helmholtz plane (IHP).[25] Other ions attracted by Coulombic forces that operate beyond the IHP, i.e., at the outer Helmholtz plane (OHP) and the diffuse layer—referred to collectively as the diffusion boundary layer (DBL)—balance the remaining charge. The ions beyond the IHP are bound more loosely to the surface and therefore can be influenced by an applied electric field.[25,28] This can produce alterations in the structure (i.e., in the region between the IHP and the shear plane) and properties of the EDL, including its compactness and the magnitude of its potential. In this work, we reveal the consequent effects on the dissolution of mineral particulates (i.e., bulk dissolution rather than dissolution in a narrow gap[20,21]) by (i) varying the solution's ionic strength (I, M), which affects the Debye length (κ^{-1}, nm), and/or (ii) application of direct current (DC) subcritical electric potential. Special focus is paid to elaborate on how electric potential may affect dissolution under conditions of surface and/or transport control. The outcomes of the work clarify the mechanisms by which external (subcritical) applied potentials affect mineral dissolution and other phenomena at the mineral−water interface such as counterion electrosorption and mineral nucleation and growth (N&G).

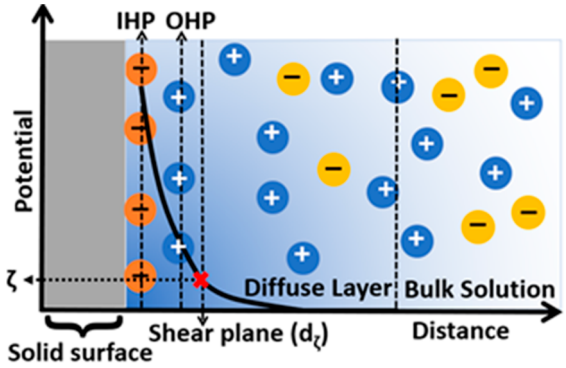

Figure 1. Schematic of the (mineral) calcite−water (solution) interface, showing the electric double layer (EDL). The inner Helmholtz plane (IHP) is composed of strongly adsorbed species, and the outer Helmholtz plane (OHP) confines the region that is composed of ions that are attracted electrostatically. The concentration of ions in the diffuse layer decreases with distance from the surface. The zeta potential (ζ) is defined as the potential difference between the OHP and the bulk solution, the latter of which is electrically neutral ($\Delta V = 0$). The ions located beyond the OHP can diffuse freely in the bulk solution.

MATERIALS AND METHODS

Materials. Natural Iceland Spar calcite and orthoclase were sourced from Ward's Science Company.[29] The bulk samples were powdered by using a ball mill and sieved through the No. 140 sieve (106 μm). The particle size distributions (PSDs) of the particulates were determined by using static light scattering (SLS, LS13-320, Beckman Coulter).[30] A mixture of isopropyl alcohol (IPA) and calcite particulates was ultrasonicated for 30 s prior to the PSD measurements to ensure that the solids are well dispersed. The particle size analysis indicates a median diameter (d_{50}) of 101.1 μm and a geometric specific surface area (SSA) of 244.9 cm^2/g (assuming spherical particles). The electrolytes used (0.001, 0.01, 0.1, and 1 M NaCl) for dissolution were prepared by adding reagent grade sodium chloride (NaCl) to Milli-Q deionized (DI) water (>18 MΩ·cm) and adjusting the pH of the solution to pH 4, 8, and 10 by using hydrochloric acid (HCl) or sodium hydroxide (NaOH). The solution pH was measured by using a benchtop pH meter (Thermo Scientific Orion Versa Star Pro) calibrated over the range $2 \leq$ pH ≤ 13 at 22 ± 1 °C.

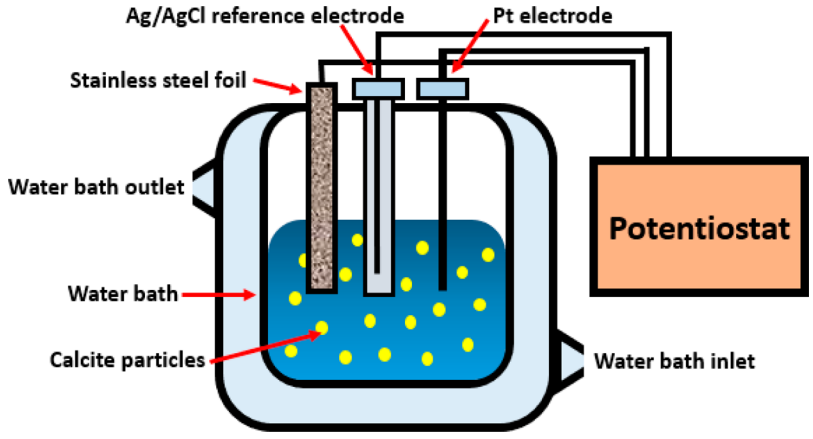

Figure 2. Illustration (not to scale) of the custom three-electrode system connected to a potentiostat. The working electrode is a Pt wire, the reference electrode is a Ag/AgCl wire in a glass tube containing 1 M KCl solution, and the counter electrode is a planar steel foil. The setup was connected to a water bath to maintain isothermal conditions during dissolution.

https://dx.doi.org/10.1021/acs.jpcc.0c04823
J. Phys. Chem. C 2020, 124, 16515−16523

Zeta Potential. Zeta potential measurements were performed by suspending 1 g of calcite particulates ($d_{50} \approx 101\ \mu m$) in 100 mL of calcite-saturated solution to minimize calcite dissolution during the measurements. A small amount (0.5 mL) of the suspension was added to 100 mL of NaCl electrolyte solutions with ionic strengths of 0.001, 0.01, 0.1, and 1 M NaCl. The test solutions were ultrasonicated for 1 min before 1.5 mL of the suspension was placed into a quartz cuvette for zeta potential measurement. Zeta potentials were measured by using a ZetaPALS (phase analysis light scattering) potential analyzer from Brookhaven Instruments Corporation that assessed the electrophoretic mobility of the particles suspended in solution.[31] In general, three measurements were obtained for each ionic strength, wherein each measurement consisting of 10 replicates was averaged to obtain representative data.

Inductively Coupled Plasma−Optical Emission Spectrometry (ICP-OES). To investigate the effect of electric potential on mineral dissolution, a custom-built three-electrode system attached to a potentiostat (VersaSTAT 4, Princeton Applied Research)[32] was used. The working electrode consisted of a platinum (Pt) wire (probe radius: 0.5 mm; length: 32 mm; CH Instruments, Inc.),[33] a reference electrode consisted of a Ag/AgCl wire (probe radius: 0.5 mm) placed in a glass Luggin capillary containing 1 M KCl solution (CH Instruments, Inc.),[33] and a counter electrode consisting of a steel foil with dimensions of 1 cm × 3 cm. The distance between the working electrode and the reference electrode was 0.5 cm, whereas the working and counter electrodes were spaced 1.0 cm apart, as shown in Figure 2.

During mineral dissolution, a 100 mL jacketed reaction beaker was connected to a recirculating water bath (Polyscience)[34] to maintain the temperature at 20, 40, or 60 ± 0.5 °C. Calcite particles (0.1 g) were dispersed in 50 mL of NaCl solution (solid-to-liquid ratio of 1:500) which was placed in the electrochemical cell. (For reference, the anodic breakdown potential of water (V_b, V) with respect to the Ag/AgCl reference electrode is expressed as $V_b = 1.23 - 0.059pH - 0.235$ at 25 °C, wherein pH refers to the pH of the immersion solution.) Thereafter, a constant potential of 0, 0.001, 0.01, 0.1, 0.2, 0.3, and 0.4 V versus the reference electrode was applied for a period of up to 12 min for calcite and 2.5 h for orthoclase. These potentials were selected to avoid pH changes induced by water's electrolysis. The initial dissolution rates of calcite and orthoclase were determined from the rate of Ca or Si release from 0 to 12 min or from 0 to 2.5 h, respectively, normalized to the initial surface area of the particulates (assuming spherical particles). The reacted solvent was collected every 3 min (i.e., 0, 3, 6, 9, and 12 min of reaction) for calcite or every 0.5 h (i.e., 0.5, 1, 1.5, 2, and 2.5 h of reaction) for orthoclase. A small quantity (~1.2 mL) of the solvent was passed through a 0.2 μm nylon syringe filter and later diluted 2 times with 5 vol % HNO_3 for analysis of concentrations of dissolved Ca and Si by using ICP-OES (PerkinElmer Avio 200) in axial view.[35] For each experimental condition, three separate measurements were performed.

For comparison, a set of control experiments (i.e., dissolution rates measured in the absence of applied potential in selected electrolyte concentrations) was conducted under native (i.e., static, potential-free) conditions. Geochemical simulations were performed using PHREEQC[36] with the pitzer.dat database, which confirmed that all solutions remained undersaturated with respect to the minerals of relevance over the entire duration of the experiment(s). For reference, the calculated saturation indices, Ω, are around −5.0 and −16.8 at the longest reaction times for calcite and orthoclase, respectively, suggesting that dissolution occurred far from equilibrium (<−12 kJ/mol and −150 to −70 kJ/mol for calcite and orthoclase, respectively).[37,38] For this reason, mineral dissolution produced an increase in the ionic strength of the solution of no more than 0.01 M at the longest reaction times.

RESULTS AND DISCUSSION

Effects of Ionic Strength on Calcite's Dissolution Rate. In general, increasing the solution's ionic strength from 0 to 1 M NaCl resulted in an increase in calcite's dissolution rate by a factor of 2.5 (see Figure 3a). Previously, calcite's

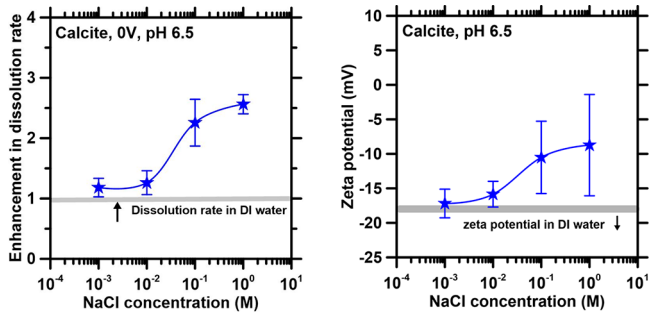

Figure 3. (a) Dissolution rate and (b) zeta potential of calcite as a function of NaCl concentration at ambient temperature. In general, both the dissolution rate and zeta potential increased with increasing NaCl concentration. For reference, calcite dissolves at a rate of 3.8×10^{-8} mol/(m^2 s) under unstirred ("static"), potential-free conditions at room temperature.

dissolution behavior in similar solutions has been observed to show a dependence on the saturation state of the solution with respect to the solute written as

$$D_r = k_d[1 - \exp(IAP/K_{sp})]^n \quad (1)$$

wherein D_r is the dissolution rate, k_d is a rate constant that depends on the solution chemistry, IAP is the ion activity product, for calcite written as $\{Ca^{2+}\}\{CO_3^{2-}\}$, K_{sp} is the solubility product (for calcite, $\log(K_{sp}) = -8.46$ at 25 °C), and n is the reaction order. The exponential term is often abbreviated by Ω, which represents the saturation state of the solute, in the solvent (also known as the undersaturation).[24] The activities of Ca^{2+} (major) and CO_3^{2-} (minor) decrease with increasing solution ionic strength as a result of their increasing extent of complexation with Cl^- and Na^+. The increase in the thermodynamic driving force that results produces an enhancement in the dissolution rate.[39] For example, calculations using PHREEQC show that the activities of Ca^{2+} and CO_3^{2-} in NaCl solutions with ionic strengths ranging between 0 and 1 M decreased from 1.11×10^{-4} to 9.45×10^{-5} for Ca^{2+} and remained around $(4.0 \pm 0.25) \times 10^{-5}$ for CO_3^{2-} at room temperature. As such, the observed increase in dissolution rates (around 2.5×) is significantly larger than that which is presumably induced by the reduction in calcite's ion activity product (reduction of 1.2×), thus implying that other dissolution-enhancing processes may be operative.

https://dx.doi.org/10.1021/acs.jpcc.0c04823
J. Phys. Chem. C 2020, 124, 16515−16523

The presence of dissolved ions is well-known to alter the thickness and structure of the EDL, as indicated via zeta potential measurements (see Figure 3), written as

$$\kappa = [\varepsilon_r \varepsilon_0 k_B T/(2e^2 I)]^{0.5} \quad (2)$$

where κ is the Debye length (nm^{-1}) ε_r and ε_0 are the relative permittivity and the permittivity of free space, respectively, k_B is Boltzmann's constant, T is the thermodynamic temperature, e is the elementary charge, and I is the ionic strength (N.B.: herein, κ < 10 nm in all cases). In general, we observe that the magnitude of the zeta potential decreases (i.e., becomes less negative) from −17.2 to −8.7 mV as the ionic strength is increased from 0.001 to 1 M. This corresponds to the compression of the EDL with increasing concentrations of Na^+ and Cl^- ions.[40,41] The large uncertainties in the zeta potential are related to uncertainties in determining the spatial distribution and concentration of the ions within the EDL.[42] Although differences in the method of measurement (e.g., streaming potential or static potential) or the source of the solute materials[43] may affect the zeta potentials, our measurements are consistent with prior literature data, e.g., that of Mahrouqi et al. (i.e., −14 mV at 0.04 M NaCl and −4 mV at 3 M NaCl).[41,44]

The (zeta) potential-determining ions for calcite are not protons (H^+) or hydroxyl ions (OH^-), as in quartz (SiO_2), for example, but instead the Ca^{2+}, CO_3^{2-}, HCO_3^-, and $H_2CO_3^0$ species.[45] At the calcite−solution interface, ions chemically interact with the surface, thereby creating surface species such as $CaOH_2^{+0.5}$, $CaOH^{-0.5}$, or $CO_3^{-0.5}$, which affects both the zeta potential and the dissolution rate (see Figure 4). The

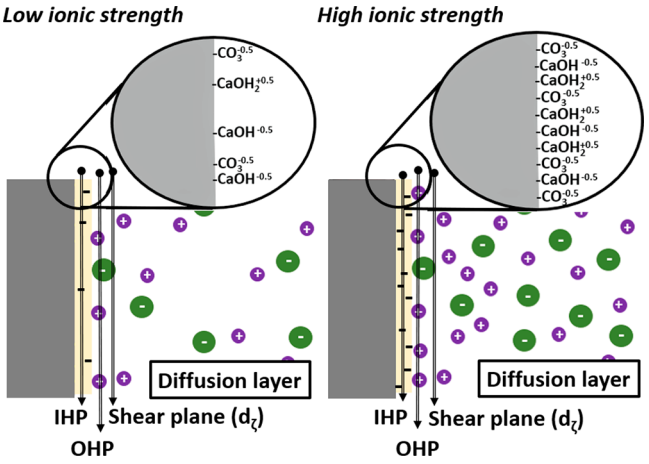

Figure 4. Schematic of a calcite surface in low and high ionic strength solutions. Ions that are specifically adsorbed on the surface at IHP (yellow region) determine the surface charge. The ions (Na^+, Cl^-) located beyond the IHP are attracted to the surface by Coulombic forces and are mobile. This model is adapted from Stipp et al. for surface speciation and Bazant et al. for the structure of EDL.[45,54] Also, shown in the schematic are Na^+ (purple), Cl^- (green), and surface-adsorbed ions layer (yellow).

crowding of anions and cations within the EDL with increasing ionic strength results in a greater degree of interaction between ions in the EDL and calcite surfaces. As a larger volume of ions is attracted to the mineral surface, the EDL compresses, thereby resulting in a higher density of reactive surface sites, especially $CO_3^{-0.5}$,[46] thereby increasing dissolution rates.[47] As such, increasing the solution's ionic strength by the addition of NaCl enhances calcite's dissolution rate on account of (1) altering (decreasing) ion activities which increases the undersaturation of the bulk solution and (2) altering (enhancing) the number of reactive surface sites at the mineral−liquid interface which facilitates dissolution.

Surface- and Transport-Controlled Dissolution. The effect of applied potential on dissolution rates was examined at I = 0.01 M over the pH range of 4−10 for calcite and pH 6.5 for orthoclase. This pH range covers calcite's dissolution including transport-controlled, mixed-kinetics, and surface-controlled regimes and the surface-controlled regime for orthoclase, a mineral that dissolves around 100× slower than calcite at T = 20 °C.[48] The zeta potentials differ by up to 10 mV over this pH range,[49] but the corresponding variation in dissolution rates, at different zeta potentials, is significantly less than the pH-related variation (i.e., >1 order of magnitude).[50] The change in dissolution rates associated with a change in the pH is primarily on account of changes in the $[H^+]$ and $[OH^-]$ ion activities in bulk solution; i.e., rather than changes in the EDL's structure in the vicinity of the mineral/water interface. At this time, it should be noted that the dissolution rate of calcite under an applied electric potential is enhanced at both acidic (pH 4) and near-neutral (pH 6.5) conditions—similarly—whereas the dissolution rate remains unaffected by applied potential at pH 10 (see Figure 5a).[51,52] For orthoclase,

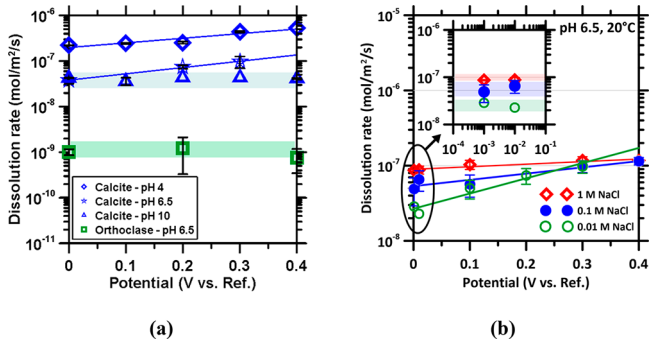

Figure 5. (a) Dissolution rates of calcite and orthoclase as a function of applied electric potential at pH 4, 6.5, and 10, showing the potential dependence of dissolution. The data are fitted by an Arrhenius-like equation of the form $D_r = k_d \exp(F_a V/RT)$. For calcite's dissolution at pH 4 and pH 6.5, $F_a/RT \approx 2.33\ V^{-1}$ (i.e., F_a = 5.78 kJ/(mol V)). No potential-induced dissolution increase was observed at pH 10 for calcite or for orthoclase. For reference, the baseline dissolution rates of calcite in the absence of applied potential at pH 4, 6.5, and pH 10 are 2.21×10^{-7}, 3.79×10^{-8}, and 4.25×10^{-8} mol/(m^2 s), respectively. (b) A "Tafel-like" plot showing the dissolution rates of calcite as a function of the applied electric potential (V) at varying ionic strengths shows greater enhancements for more dilute solutions. The data were fitted by using eq 3 across all ionic strengths.

across all solution pH's its dissolution rates are unaffected by the applied potential—an important observation given that orthoclase is known to dissolve under surface control across the pH range studied herein,[53] as will be discussed below.

A previous study has shown that the ion adsorption rate on solute surfaces is affected by electric potential, especially for conductive materials.[55] On the other hand, counterion sorption to mineral surfaces has been observed to induce changes in mineral dissolution rates by up to 1 order of magnitude.[56,57] Besides ion adsorption, applying an electric potential within an electrolytic solution could also increase the

https://dx.doi.org/10.1021/acs.jpcc.0c04823
J. Phys. Chem. C 2020, 124, 16515−16523

rate of ion transport, especially at interfaces, which could affect mineral dissolution rates.[55,58] Herein, significant enhancements in dissolution rates when a potential is applied, e.g., for calcite, are observed—under isothermal conditions—only under conditions of mass transport (pH 4) and mixed kinetic control (pH 6.5)[13,51,59] but not when dissolution is interface-controlled (pH 10).[15,60] Significantly, the recent work of Dobbs et al.[21] shows that electric potential has limited, if any, effect on bulk dissolution rates (i.e., at large surface-to-surface separations when the EDLs of neighboring solute surfaces do not interact) under surface-controlled conditions. This may suggest that an applied potential has a greater influence on ion transport than on ion adsorption, thus affecting mineral dissolution rates only under conditions of mass-transport control.[22]

A particularly interesting observation is that the dissolution rate data, in Figure 5, under conditions of electric stimulations is robustly fitted by an equation of the form

$$D_r = k_d \exp(F_a V/RT) \tag{3}$$

where F_a is the apparent activation factor of dissolution under conditions of electric stimulation and V is the applied potential. This fitting suggests an Arrhenius-like "Butler–Volmer" process that implicates an electrochemical origin of calcite's dissolution enhancement that depends on the solution chemistry and, most significantly, on the mobility of ions, e.g., in the region beyond the IHP and propagating into the bulk solution.

Assuming mass conservation at the mineral–water interface, the relationship between the flux of an aqueous species (j), which describes ion transport, and the dissolution rate (D_R) is given by[61]

$$j = \frac{1}{s}\alpha D_R \tag{4}$$

where s is the cross-sectional area perpendicular to the transport direction and α is a dimensionless stoichiometric coefficient (for calcite dissolution the coefficient takes a value of unity). Ion motion induced by electric potential ("electro-migration") can be estimated by using the Nernst–Planck equation:

$$j = -D\left[\nabla c + \frac{zF}{RT}c(\nabla V)\right] \tag{5}$$

where D is the ion diffusivity, ∇V is the gradient of the electric potential (i.e., electric field), z is the valence of ionic species, F is the Faraday constant, and T is the temperature. The aqueous species flux (j) is determined by both the gradient of ion concentration and the electric field (i.e., the first and the second term on the right-hand side of eq 5, respectively). The second term is added to represent the electrostatic force that is caused by the external electric potential.[58] The Nernst–Planck model suggests that, expectedly, the electric field disturbs the ionic flux and facilitates ion migration toward oppositely charged electrodes. As demonstrated by the measured dissolution enhancement (see Figure 5), such flux perturbation induced by the electric field elevates the total ion flux and therefore the mineral dissolution rate (i.e., $j \propto D_R \propto \nabla V$). Equation 3 assumes that the fluid velocity is zero (i.e., only the dissolved ions move) and that the external electric potential is at steady state, as applicable to this study.[58]

The contribution of the electric field to ion transport can be analogously compared to the effects of promoting solution convection as induced in rotating plate tests.[14] Under mass-transfer control, calcite's dissolution rate is limited by $[H^+]$ transport and the pH of the bulk solution according to[14]

$$\log(D_R) = \log\left(\frac{k_t k_{H^+}\gamma_{H^+}}{k_t + k_{H^+}\gamma_{H^+}}\right) - \mathrm{pH} \tag{6}$$

where k_t is the H^+ transport rate constant, γ_{H^+} is the proton's activity coefficient,[62] and k_{H^+} is the H^+–calcite reaction constant ($k = 9.5 \times 10^{-6}$ 1/cm^2·s).[52] Therefore, k_t can be estimated by using the data presented in Figure 5, and in addition, an equivalent rotational velocity (ω)—for the solvent—can be obtained whereby

$$k_t = 0.6 D^{2/3}\nu^{-1/6}\omega^{1/2} \tag{7}$$

where D is the proton diffusivity ($D = 3.0 \times 10^{-5}$ cm^2/s)[14] and ν is the solution's viscosity (ν = 1310.92 cm^2/s).[63] This analysis indicates that applied potential induces stimulation of proton transport that is equivalent to a 40× enhancement in the solution's angular (rotational) velocity in the proximity of the solute. Taken together, this suggests that the net enhancement of calcite's dissolution is produced by enhancing the motion of hydrated solute (and solvent) species in solution.

Effect of Solution Viscosity and Temperature. The extent to which ion transport is affected by electric potential depends on the ionic strength, solution viscosity, and solution temperature. Hence, in Figure 5b, the measured calcite dissolution rates at pH 6.5 and 0.01 M < I < 1 M are plotted as a function of the applied potential following eq 3. It is noted that for a given ionic strength calcite dissolution rates were effectively unchanged for applied potentials between 0.001 and 0.01 V and increased dramatically at V > 0.1 V, particularly at lower ionic strengths. Of course, the ionic strength affects the solvent's viscosity,[63] which in turn affects the rate of ion transport, i.e., an ion's diffusivity, D, as described by the Stokes–Einstein relation:[64]

$$D = \frac{k_B T}{6\pi\eta_s R} \tag{8}$$

where k_B is Boltzmann's constant (1.38×10^{-23} m^2 kg/(s^2 K)), η_s is the solution's viscosity ($\eta_s = \eta/\eta_0$, η_0 = viscosity of pure water), R is the solute radius (i.e., the average of the hydrated radii of Ca^{2+} and CO_3^{2-} $\approx$ 0.296 nm and $[H^+]$ $\approx$ 0.282 nm),[65−67] and T is the temperature. The viscosity data of Ozbek et al.[63] show that the solution's viscosity (η_r) relative to pure water increases with NaCl molarity (M) according to $\eta_r = 1 + A\sqrt{M} + BM + CM^2$, where A, B, and C are temperature-dependent coefficients. Thus, increasing I from 0.01 to 1 M is expected to increase the solvent's viscosity by about 1.1×. As such, the calculated diffusivities of calcite's constituent ions and H^+ in solution would change proportionately (N.B.: it is reasonable to neglect the change in the ionic strength associated with calcite's dissolution, which is around 0.01 M, producing an enhancement of 0.14% in solvent viscosity). This clarifies that the change in the solution's viscosity only slightly affects the extent of dissolution rate enhancement.

Returning to Figure 5b, the fitting of eq 6 to the experimental data indicates that F_a scales as 11.7 kJ/(mol V)

https://dx.doi.org/10.1021/acs.jpcc.0c04823
J. Phys. Chem. C 2020, 124, 16515−16523

(0.01 M) > 4.0 kJ/(mol V) (0.1 M) > 1.4 kJ/(mol V) (1 M) in order of increasing ionic strength. This scaling, for a process linked to ion transport, is unsurprising as ion mobility and transport, not only in bulk solution but also at the solid−solution interface, are known to be strongly affected by the ionic strength, i.e., due to an increase in ion−ion interactions in concentrated solutions.[68] Ion−ion correlations hinder the movement of ions; therefore, herein the dissolution enhancements decrease with ionic strength for the same applied potential. Nevertheless, the observed increase in dissolution rates with applied potential (see Figure 5) suggests that, in essence, F_aV quantifies the extent by which application of an electric potential reduces the (net) apparent activation energy of mineral dissolution at a given isothermal temperature. To ascertain this assumption, calcite's dissolution rates were quantified across a range of temperatures, both under potential-free ("native") and electrically stimulated conditions for a single solution composition (pH 6.5, 0.01 M NaCl). Why? To examine the hypothesis that F_aV represents the easing/reduction of the apparent activation energy of mineral dissolution (E_{ad}, kJ/mol). First, it was observed that calcite's dissolution rate increases by nearly 1 order of magnitude as the temperature is increased from 20 to 60 °C[13] (Figure 6a), in the absence of applied potential under static conditions.[37] Interestingly, while applied potential does indeed increase calcite's dissolution rate, the extent of the dissolution enhancement diminishes with increasing temperature, such that the dissolution rates at 60 °C are nearly equivalent, whether electric stimulation is applied or not. This may imply an effect that is related to the ionic mobility (diffusivity), which enhances with temperature. For example, the ionic diffusivity in bulk solution increases by 14% over this temperature range, and that could be much larger in regions such as the DBL—a change which at 60 °C could readily change the rate-limiting step of dissolution from transport to surface control.[13]

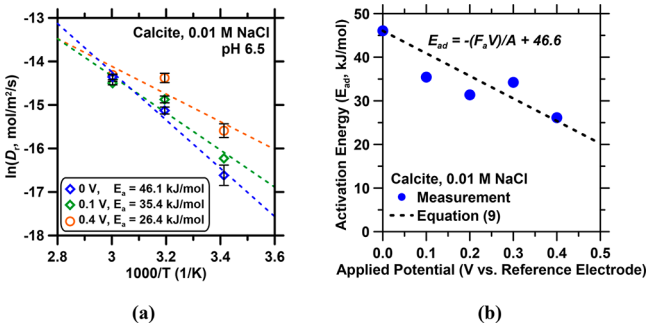

Figure 6. (a) Arrhenius plot showing calcite's dissolution rates as a function of the inverse temperature for different applied potentials ranging from 0 to 0.4 V. The data are fitted to an equation of the form $D_r = k_d \exp(-E_{ad}/RT)$, where E_{ad} is the *apparent* activation energy of the (net) mineral dissolution reaction. It is seen that greater rate enhancements are induced at lower temperatures. The solvent pH is measured to be around 8.2−8.4 (pH units) at the end of the experiment. (b) Reduction in the apparent activation energy (E_{ad}) of calcite dissolution with applied electric potential. The data are fitted to eq 9, where F_a = 11.7 kJ/(mol V) and A is a fitting variable that represents the electrochemical cell's geometry/configuration that affects the electric field and the solution conditions including its chemistry and ionic composition (0.23, unitless).

Second, Arrhenius analysis of calcite dissolution rates at different isothermal conditions in the absence of applied potential, far from saturation, indicates an apparent activation energy of dissolution, E_{ad} = 47 ± 3.3 kJ/mol, which is in good agreement with prior data.[13,52] Interestingly, the activation energy of dissolution is observed to systematically decrease, linearly, as the electric potential is increased, decreasing to 26 ± 2.3 kJ/mol at an applied potential of 0.4 V (see Figure 6b). Third, it is noted that the decrease in the apparent activation energy of mineral dissolution is proportional to the extent by which application of an electrical stimulus enhances the dissolution process as quantified by the equation

$$E_{ad} = -(F_aV)/A + 46.6 \quad (9)$$

This reduction in the thermodynamic barrier for dissolution suggests a fundamental change in the reaction mechanism.

As such it is postulated that application of an electric field enhances dissolution by accelerating ion transport in the region beyond the IHP, i.e., in the OHP and in the diffuse layer, such that while the surface speciation on the calcite surface remains broadly unaffected (e.g., although the ionic, and particularly, the proton distribution may be somewhat altered, within the IHP), the rate of ingress/egress of solvent/solute ions (e.g., H^+, Ca^{2+}, and carbonate/bicarbonate species)—exchanging with the bulk solution—is accelerated, thereby enhancing calcite's dissolution rate. This enhanced ingress/egress of ions in the interfacial zone acts to reduce the thermodynamic barrier of the net dissolution reaction, and this reduction is quantified by F_aV as shown in Figure 5. As such, as calcite dissolves, the local surface undersaturation decreases as the dissolved ions increasingly accumulate in the diffusion-boundary layer (DBL; i.e., the broad region between the IHP and the bulk solution[69,70]) and within etch pits that form on the surface. An applied potential facilitates ion movement across the DBL and out of the etch pits into bulk solution, thereby sustaining a high(er) local undersaturation. This mechanism of potential-induced surface *desaturation* reduces the energy barrier for etch pit nucleation,[16] thus further activating pit formation. For instance, Naviaux et al.[71] have shown that with an increasing undersaturation the etch pits nucleation mechanism can change from preexisting kinks assisted to defect assisted (e.g., point defects and edge dislocations); with increased undersaturation, calcite eventually adapts a homogeneous dissolution mechanism, which promotes layer-by-layer dissolution. Such a transition of etch-pit nucleation sites has been observed to be accompanied by the changes in the activation energy[71] (see Figure 6a). This explains the observation that under transport and mixed-mode control an applied potential reduces the activation energy of dissolution (Figure 6b). This also indicates that the nature of defects on the mineral surface, which are initially present, would strongly affect its dissolution behavior ("kinetics") in any solution environment, although to lesser or greater extents. On the other hand, when dissolution is purely surface controlled, as is the case of orthoclase, or for calcite dissolution at hyperalkaline conditions, the thermodynamics of dissolution, and ion transport, more broadly, are unaffected by the applied potential. Therefore, calcite dissolution at pH ≥ 10 and orthoclase dissolution are unaffected by electric stimulation.

SUMMARY AND CONCLUSIONS

This study demonstrates that subcritical electric potential has a significant effect on mineral dissolution under conditions of transport control at isothermal conditions, e.g., for calcite at pH < 8. This is so even in circumstances wherein the electric

https://dx.doi.org/10.1021/acs.jpcc.0c04823
J. Phys. Chem. C 2020, 124, 16515−16523

double layers (EDLs) of particles do not overlap, and very large surface-to-surface separations (i.e., $\gg\kappa$) remain. In the absence of electrolysis-induced acidification, an applied electric potential alters ion ingress and egress ("transport") rates into and out of the diffusion-boundary layer (DBL), thereby producing enhancements in dissolution when the process is transport-controlled. The extent of enhancement that results depends on the solution's characteristics, particularly its ionic strength and composition. When dissolution is surface-controlled, e.g., calcite dissolution at high pH and orthoclase dissolution at near-neutral pH, the applied electric potential is unable to affect mineral dissolution rates. These observations are explained on the basis that while subcritical applied potentials do not alter ion adsorption and speciation at the mineral−solvent interface, the applied potential affects the mobility of ions, thereby enhancing their movement across the diffusion boundary layer (DBL; i.e., the broad region between the IHP and bulk solution). The increase in dissolution rates that results is quantified by an apparent activation energy of dissolution under conditions of electric stimulation given by the product F_aV, which indicates a Butler−Volmer-type process of dissolution stimulation. Furthermore, the apparent activation energy of calcite's dissolution decreases with increasing electric potential, in proportion to F_aV and as a function of the solution conditions and cell geometry. This suggests a fundamental shift in the reaction mechanism that is caused by electric stimulation. Taken together, the outcomes of this work offer new insights into the use of electrochemical stimulation for enhancing mineral dissolution rates for artificial ocean alkalinization[5] and affecting nucleation and growth (N&G) processes with special focus on applications including soil remediation, materials synthesis, nuclear waste disposal, and chemical−mechanical polishing.

AUTHOR INFORMATION

Corresponding Author

Gaurav Sant − *Laboratory for the Chemistry of Construction Materials (LC2), Department of Civil and Environmental Engineering, Institute for Carbon Management (ICM), Department of Materials Science and Engineering, and California Nanosystems Institute, University of California, Los Angeles, Los Angeles, California 90095, United States;* orcid.org/0000-0002-1124-5498; Phone: (310) 206-3084; Email: gsant@ucla.edu

Authors

Yi-Hsuan Hsiao − *Laboratory for the Chemistry of Construction Materials (LC2), Department of Civil and Environmental Engineering, University of California, Los Angeles, Los Angeles, California 90095, United States*

Xin Chen − *Laboratory for the Chemistry of Construction Materials (LC2), Department of Civil and Environmental Engineering and Institute for Carbon Management (ICM), University of California, Los Angeles, Los Angeles, California 90095, United States;* orcid.org/0000-0003-3273-4431

Erika Callagon La Plante − *Laboratory for the Chemistry of Construction Materials (LC2), Department of Civil and Environmental Engineering and Institute for Carbon Management (ICM), University of California, Los Angeles, Los Angeles, California 90095, United States; Department of Materials Science and Engineering, University of Texas at Arlington, Arlington, Texas 76019, United States;* orcid.org/0000-0002-5273-9523

Aditya Kumar − *Department of Materials Science and Engineering, Missouri University of Science and Technology, Rolla, Missouri 65409, United States;* orcid.org/0000-0001-7550-8034

Mathieu Bauchy − *Institute for Carbon Management (ICM) and Physics of Amorphous and Inorganic Solids Laboratory (PARISlab), Department of Civil and Environmental Engineering, University of California, Los Angeles, Los Angeles, California 90095, United States;* orcid.org/0000-0003-4600-0631

Dante Simonetti − *Institute for Carbon Management (ICM) and Department of Chemical and Biomolecular Engineering, University of California, Los Angeles, Los Angeles, California 90095, United States;* orcid.org/0000-0002-5708-460X

David Jassby − *Institute for Carbon Management (ICM) and Water Technologies Laboratory, Department of Civil and Environmental Engineering, University of California, Los Angeles, Los Angeles, California 90095, United States;* orcid.org/0000-0002-2133-2536

Jacob Israelachvili − *Interfacial Sciences Laboratory, Department of Chemical Engineering, University of California, Santa Barbara, Santa Barbara, California 93106, United States;* orcid.org/0000-0001-8915-8741

Complete contact information is available at: https://pubs.acs.org/10.1021/acs.jpcc.0c04823

Author Contributions

Y.-H.H. and X.C. both contributed equally to this work.

Notes

The authors declare no competing financial interest.

J.I.: deceased (19 August 1944−20 September 2018).

ACKNOWLEDGMENTS

The authors acknowledge financial support for this research provisioned by the U.S. Department of Energy's (i) Office of Fossil Energy (DE-FE0029825 and DE-FE0031705) and (ii) Advanced Research Projects Agency-Energy (ARPA-e: DE-AR-0001147) and the U.S. National Science Foundation (DMREF: 1922167). The contents of this paper reflect the views and opinions of the authors, who are responsible for the accuracy of data presented herein, and do not reflect the views and/or policies of the funding agency, nor do the contents constitute a specification, standard or regulation.

REFERENCES

(1) Morse, J. W.; Arvidson, R. S. The Dissolution Kinetics of Major Sedimentary Carbonate Minerals. *Earth-Sci. Rev.* **2002**, *58* (1), 51−84.

(2) Hales, B.; Emerson, S. Evidence in Support of First-Order Dissolution Kinetics of Calcite in Seawater. *Earth Planet. Sci. Lett.* **1997**, *148* (1), 317−327.

(3) Schnoor, J. L.; Stumm, W. The Role of Chemical Weathering in the Neutralization of Acidic Deposition. *Schweiz. Z. Hydrol.* **1986**, *48* (2), 171−195.

(4) Köhler, P.; Hartmann, J.; Wolf-Gladrow, D. A. Geoengineering Potential of Artificially Enhanced Silicate Weathering of Olivine. *Proc. Natl. Acad. Sci. U. S. A.* **2010**, *107* (47), 20228−20233.

(5) Hartmann, J.; West, A. J.; Renforth, P.; Köhler, P.; De La Rocha, C. L.; Wolf-Gladrow, D. A.; Dürr, H. H.; Scheffran, J. Enhanced Chemical Weathering as a Geoengineering Strategy to Reduce Atmospheric Carbon Dioxide, Supply Nutrients, and Mitigate Ocean Acidification. *Rev. Geophys.* **2013**, *51* (2), 113−149.

(6) Xia, C.; Cai, Y.; Ma, Y.; Wang, B.; Zhang, W.; Karlsson, M.; Wu, Y.; Zhu, B. Natural Mineral-Based Solid Oxide Fuel Cell with Heterogeneous Nanocomposite Derived from Hematite and Rare-

Earth Minerals. *ACS Appl. Mater. Interfaces* **2016**, *8* (32), 20748−20755.
(7) Wu, Y.; Xia, C.; Zhang, W.; Yang, X.; Bao, Z. Y.; Li, J. J.; Zhu, B. Natural Hematite for Next-Generation Solid Oxide Fuel Cells. *Adv. Funct. Mater.* **2016**, *26* (6), 938−942.
(8) Wu, Y.; Liu, L.; Yu, X.; Zhang, J.; Li, L.; Yan, C.; Zhu, B. Natural Hematite Ore Composited with ZnO Nanoneedles for Energy Applications. *Composites, Part B* **2018**, *137*, 178−183.
(9) López-Vizcaíno, R.; dos Santos, E. V.; Yustres, A.; Rodrigo, M. A.; Navarro, V.; Martínez-Huitle, C. A. Calcite Buffer Effects in Electrokinetic Remediation of Clopyralid-Polluted Soils. *Sep. Purif. Technol.* **2019**, *212*, 376−387.
(10) Mishra, S. K. The Electrokinetics of Apatite and Calcite in Inorganic Electrolyte Environment. *Int. J. Miner. Process.* **1978**, *5* (1), 69−83.
(11) Amankonah, J. O.; Somasundaran, P. Effects of Dissolved Mineral Species on the Electrokinetic Behavior of Calcite and Apatite. *Colloids Surf.* **1985**, *15*, 335−353.
(12) Ellis, L. D.; Badel, A. F.; Chiang, M. L.; Park, R. J.-Y.; Chiang, Y.-M. Toward Electrochemical Synthesis of Cement—An Electrolyzer-Based Process for Decarbonating CaCO3 While Producing Useful Gas Streams. *Proc. Natl. Acad. Sci. U. S. A.* **2020**, *117*, 12584.
(13) Sjöberg, E. L.; Rickard, D. T. Temperature Dependence of Calcite Dissolution Kinetics between 1 and 62°C at PH 2.7 to 8.4 in Aqueous Solutions. *Geochim. Cosmochim. Acta* **1984**, *48* (3), 485−493.
(14) Alkattan, M.; Oelkers, E. H.; Dandurand, J.-L.; Schott, J. An Experimental Study of Calcite and Limestone Dissolution Rates as a Function of PH from − 1 to 3 and Temperature from 25 to 80°C. *Chem. Geol.* **1998**, *151* (1), 199−214.
(15) Sjöberg, E. L.; Rickard, D. T. Calcite Dissolution Kinetics: Surface Speciation and the Origin of the Variable PH Dependence. *Chem. Geol.* **1984**, *42* (1), 119−136.
(16) Teng, H. H. Controls by Saturation State on Etch Pit Formation during Calcite Dissolution. *Geochim. Cosmochim. Acta* **2004**, *68* (2), 253−262.
(17) Ruiz-Agudo, E.; Kowacz, M.; Putnis, C. V.; Putnis, A. The Role of Background Electrolytes on the Kinetics and Mechanism of Calcite Dissolution. *Geochim. Cosmochim. Acta* **2010**, *74* (4), 1256−1267.
(18) Jones, C. E.; Unwin, P. R.; Macpherson, J. V. In Situ Observation of the Surface Processes Involved in Dissolution from the Cleavage Surface of Calcite in Aqueous Solution Using Combined Scanning Electrochemical−Atomic Force Microscopy (SECM-AFM). *ChemPhysChem* **2003**, *4* (2), 139−146.
(19) McGeouch, C.-A.; Peruffo, M.; Edwards, M. A.; Bindley, L. A.; Lazenby, R. A.; Mbogoro, M. M.; McKelvey, K.; Unwin, P. R. Quantitative Localized Proton-Promoted Dissolution Kinetics of Calcite Using Scanning Electrochemical Microscopy (SECM). *J. Phys. Chem. C* **2012**, *116* (28), 14892−14899.
(20) Kristiansen, K.; Valtiner, M.; Greene, G. W.; Boles, J. R.; Israelachvili, J. N. Pressure Solution−The Importance of the Electrochemical Surface Potentials. *Geochim. Cosmochim. Acta* **2011**, *75* (22), 6882−6892.
(21) Dobbs, H. A.; Degen, G. D.; Berkson, Z. J.; Kristiansen, K.; Schrader, A. M.; Oey, T.; Sant, G.; Chmelka, B. F.; Israelachvili, J. N. Electrochemically Enhanced Dissolution of Silica and Alumina in Alkaline Environments. *Langmuir* **2019**, *35* (48), 15651−15660.
(22) Dreybrodt, W.; Buhmann, D. A Mass Transfer Model for Dissolution and Precipitation of Calcite from Solutions in Turbulent Motion. *Chem. Geol.* **1991**, *90* (1), 107−122.
(23) Barton, P.; Vatanatham, T. Kinetics of Limestone Neutralization of Acid Waters. 5.
(24) Rickard, D.; Sjoeberg, E. L. Mixed Kinetic Control of Calcite Dissolution Rates. *Am. J. Sci.* **1983**, *283* (8), 815−830.
(25) Hunter, R. J. *Zeta Potential in Colloid Science: Principles and Applications*; Academic Press: 2013.
(26) Zhao, C.; Yang, C. Advances in Electrokinetics and Their Applications in Micro/Nano Fluidics. *Microfluid. Nanofluid.* **2012**, *13* (2), 179−203.
(27) Thompson, D. W.; Pownall, P. G. Surface Electrical Properties of Calcite. *J. Colloid Interface Sci.* **1989**, *131* (1), 74−82.
(28) Delgado, A. V.; González-Caballero, F.; Hunter, R. J.; Koopal, L. K.; Lyklema, J. Measurement and Interpretation of Electrokinetic Phenomena. *J. Colloid Interface Sci.* **2007**, *309* (2), 194−224.
(29) https://www.Wardsci.Com/Store/ (accessed on: 07/01/2020).
(30) https://www.Beckmancoulter.com/ (accessed on: 07/01/2020).
(31) https://www.Brookhaveninstruments.com/ (accessed on: 07/01/2020).
(32) https://www.Ameteksi.Com/Brands/Princetonappliedresearch (accessed on: 07/01/2020).
(33) https://www.Chinstruments.com/ (accessed on: 07/01/2020).
(34) https://www.Polyscience.com/ (accessed on: 07/01/2020).
(35) https://www.perkinelmer.com/ (accessed on: 07/01/2020).
(36) Parkhurst, D. L.; Appelo, C. A. J. Description of Input and Examples for PHREEQC Version 3—a Computer Program for Speciation, Batch-Reaction, One-Dimensional Transport, and Inverse Geochemical Calculations. *US Geol. Surv. Technol. Methods Book* **2013**, *6*, 497.
(37) Xu, J.; Fan, C.; Teng, H. H. Calcite Dissolution Kinetics in View of Gibbs Free Energy, Dislocation Density, and PCO_2. *Chem. Geol.* **2012**, *322*−*323*, 11−18.
(38) Hellmann, R.; Tisserand, D. Dissolution Kinetics as a Function of the Gibbs Free Energy of Reaction: An Experimental Study Based on Albite Feldspar. *Geochim. Cosmochim. Acta* **2006**, *70* (2), 364−383.
(39) Buhmann, D.; Dreybrodt, W. Calcite Dissolution Kinetics in the System H_2O—CO_2—CaCO3 with Participation of Foreign Ions. *Chem. Geol.* **1987**, *64* (1), 89−102.
(40) Jaafar, M. Z.; Vinogradov, J.; Jackson, M. D. Measurement of Streaming Potential Coupling Coefficient in Sandstones Saturated with High Salinity NaCl Brine. *Geophys. Res. Lett.* **2009**, DOI: 10.1029/2009GL040549.
(41) Al Mahrouqi, D.; Vinogradov, J.; Jackson, M. D. Zeta Potential of Artificial and Natural Calcite in Aqueous Solution. *Adv. Colloid Interface Sci.* **2017**, *240*, 60−76.
(42) Coday, B. D.; Luxbacher, T.; Childress, A. E.; Almaraz, N.; Xu, P.; Cath, T. Y. Indirect Determination of Zeta Potential at High Ionic Strength: Specific Application to Semipermeable Polymeric Membranes - ScienceDirect. *J. Membr. Sci.* **2015**, *478*, 58−64.
(43) Moulin, P.; Roques, H. Zeta Potential Measurement of Calcium Carbonate. *J. Colloid Interface Sci.* **2003**, *261* (1), 115−126.
(44) Al Mahrouqi, D.; Vinogradov, J.; Jackson, M. D. Temperature Dependence of the Zeta Potential in Intact Natural Carbonates. *Geophys. Res. Lett.* **2016**, *43* (22), 11,578−11,587.
(45) Stipp, S. L. S. Toward a Conceptual Model of the Calcite Surface: Hydration, Hydrolysis, and Surface Potential. *Geochim. Cosmochim. Acta* **1999**, *63* (19), 3121−3131.
(46) Perassi, I.; Borgnino, L. Adsorption and Surface Precipitation of Phosphate onto CaCO3−Montmorillonite: Effect of PH, Ionic Strength and Competition with Humic Acid. *Geoderma* **2014**, *232*−*234*, 600−608.
(47) Van Cappellen, P.; Charlet, L.; Stumm, W.; Wersin, P. A Surface Complexation Model of the Carbonate Mineral-Aqueous Solution Interface. *Geochim. Cosmochim. Acta* **1993**, *57* (15), 3505−3518.
(48) Blake, R. E.; Walter, L. M. Kinetics of Feldspar and Quartz Dissolution at 70−80°C and near-Neutral PH: Effects of Organic Acids and NaCl. *Geochim. Cosmochim. Acta* **1999**, *63* (13), 2043−2059.
(49) Siffert, D.; Fimbel, P. Parameters Affecting the Sign and Magnitude of the Eletrokinetic Potential of Calcite. *Colloids Surf.* **1984**, *11* (3), 377−389.
(50) Arvidson, R. S.; Ertan, I. E.; Amonette, J. E.; Luttge, A. Variation in Calcite Dissolution Rates:: A Fundamental Problem? *Geochim. Cosmochim. Acta* **2003**, *67* (9), 1623−1634.

(51) Brantley, S. L. Kinetics of Mineral Dissolution. In *Kinetics of Water-Rock Interaction*; Brantley, S. L., Kubicki, J. D., White, A. F., Eds.; Springer: New York, 2008; pp 151−210.
(52) Sjöberg, E. L. A Fundamental Equation for Calcite Dissolution Kinetics. *Geochim. Cosmochim. Acta* **1976**, *40* (4), 441−447.
(53) Fenter, P.; Zapol, P.; He, H.; Sturchio, N. C. On the Variation of Dissolution Rates at the Orthoclase (0 0 1) Surface with PH and Temperature. *Geochim. Cosmochim. Acta* **2014**, *141*, 598−611.
(54) Bazant, M. Z.; Kilic, M. S.; Storey, B. D.; Ajdari, A. Towards an Understanding of Induced-Charge Electrokinetics at Large Applied Voltages in Concentrated Solutions. *Adv. Colloid Interface Sci.* **2009**, *152* (1), 48−88.
(55) Ngankam, A. P.; Van Tassel, P. R. Continuous Polyelectrolyte Adsorption under an Applied Electric Potential. *Proc. Natl. Acad. Sci. U. S. A.* **2007**, *104* (4), 1140−1145.
(56) Biber, M. V.; dos Santos Afonso, M.; Stumm, W. The Coordination Chemistry of Weathering: IV. Inhibition of the Dissolution of Oxide Minerals. *Geochim. Cosmochim. Acta* **1994**, *58* (9), 1999−2010.
(57) Hsiao, Y.-H.; La Plante, E. C.; Krishnan, N. A.; Dobbs, H. A.; Le Pape, Y.; Neithalath, N.; Bauchy, M.; Israelachvili, J.; Sant, G. Role of Electrochemical Surface Potential and Irradiation on Garnet-Type Almandine's Dissolution Kinetics. *J. Phys. Chem. C* **2018**, *122* (30), 17268−17277.
(58) Kirby, B. J. *Micro- and Nanoscale Fluid Mechanics: Transport in Microfluidic Devices*; Cambridge University Press: 2010.
(59) Plummer, L. N.; Wigley, T. M. L. The Dissolution of Calcite in CO_2-Saturated Solutions at 25°C and 1 atm Total Pressure. *Geochim. Cosmochim. Acta* **1976**, *40* (2), 191−202.
(60) Chou, L.; Garrels, R. M.; Wollast, R. Comparative Study of the Kinetics and Mechanisms of Dissolution of Carbonate Minerals. *Chem. Geol.* **1989**, *78* (3), 269−282.
(61) Murphy, W. M.; Oelkers, E. H.; Lichtner, P. C. Surface Reaction versus Diffusion Control of Mineral Dissolution and Growth Rates in Geochemical Processes. *Chem. Geol.* **1989**, *78* (3−4), 357−380.
(62) Capone, S.; De Robertis, A.; De Stefano, C.; Sammartano, S.; Scarcella, R. Ionic Strength Dependence of Formation Constants—X: Proton Activity Coefficients at Various Temperatures and Ionic Strengths and Their Use in the Study of Complex Equilibria. *Talanta* **1987**, *34* (6), 593−598.
(63) Ozbek, H.; Fair, J. A.; Phillips, S. L. *Viscosity of Aqueous Solium Chloride Solutions from 0−150* °C; No. LBL-5931; Lawrence Berkeley National Lab. (LBNL): Berkeley, CA, 1977.
(64) Edward, J. T. Molecular Volumes and the Stokes-Einstein Equation. *J. Chem. Educ.* **1970**, *47* (4), 261.
(65) Simoes, M. C.; Hughes, K. J.; Ingham, D. B.; Ma, L.; Pourkashanian, M. Estimation of the Thermochemical Radii and Ionic Volumes of Complex Ions. *Inorg. Chem.* **2017**, *56* (13), 7566−7573.
(66) Railsback, L. B. *Some Fundamentals of Mineralogy and Geochemistry* http://railsback.org/FundamentalsIndex.html#Solutions (accessed Sept 12, 2019).
(67) Paul, S.; Choi, K. S.; Lee, D. J.; Sudhagar, P.; Kang, Y. S. Factors Affecting the Performance of Supercapacitors Assembled with Polypyrrole/Multi-Walled Carbon Nanotube Composite Electrodes. *Electrochim. Acta* **2012**, *78*, 649−655.
(68) Chowdhuri, S.; Chandra, A. Molecular Dynamics Simulations of Aqueous NaCl and KCl Solutions: Effects of Ion Concentration on the Single-Particle, Pair, and Collective Dynamical Properties of Ions and Water Molecules. *J. Chem. Phys.* **2001**, *115* (8), 3732−3741.
(69) Liu, Z.; Dreybrod, W. Dissolution Kinetics of Calcium Carbonate Minerals in H_2O— CO_2 Solutions in Turbulent Flow: The Role of the Diffusion Boundary Layer and the Slow Reaction H_2O+ CO_2→ H++ HCO3−. *Geochim. Cosmochim. Acta* **1997**, *61* (14), 2879−2889.
(70) Puerta-Falla, G.; Balonis, M.; Falzone, G.; Bauchy, M.; Neithalath, N.; Sant, G. Monovalent Ion Exchange Kinetics of Hydrated Calcium-Alumino Layered Double Hydroxides. *Ind. Eng. Chem. Res.* **2017**, *56* (1), 63−74.
(71) Naviaux, J. D.; Subhas, A. V.; Rollins, N. E.; Dong, S.; Berelson, W. M.; Adkins, J. F. Temperature Dependence of Calcite Dissolution Kinetics in Seawater. *Geochim. Cosmochim. Acta* **2019**, *246*, 363−384.

https://dx.doi.org/10.1021/acs.jpcc.0c04823
J. Phys. Chem. C 2020, 124, 16515−16523